

# SCIENTIFIC REPORTS



OPEN

## Elemental and Mineralogical Composition of the Western Andean Snow (18°S–41°S)

Juan A. Alfonso<sup>1,2</sup>, Raul R. Cordero<sup>1</sup>, Penny M. Rowe<sup>1,3</sup>, Steven Neshyba<sup>4</sup>, Gino Casassa<sup>5,6</sup>, Jorge Carrasco<sup>6</sup>, Shelley MacDonell<sup>7</sup>, Fabrice Lambert<sup>8,9</sup>, Jaime Pizarro<sup>1</sup>, Francisco Fernandez<sup>10</sup>, Sarah Feron<sup>1,11</sup>, Alessandro Damiani<sup>1,12</sup>, Pedro Llanillo<sup>1</sup>, Edgardo Sepulveda<sup>1</sup>, Jose Jorquera<sup>1</sup>, Belkis Garcia<sup>2</sup>, Juan M. Carrera<sup>2</sup>, Pedro Oyola<sup>13</sup> & Choong-Min Kang<sup>14</sup>

The snowpack is an important source of water for many Andean communities. Because of its importance, elemental and mineralogical composition analysis of the Andean snow is a worthwhile effort. In this study, we conducted a chemical composition analysis (major and trace elements, mineralogy, and chemical enrichment) of surface snow sampled at 21 sites across a transect of about 2,500 km in the Chilean Andes (18–41°S). Our results enabled us to identify five depositional environments: (i) sites 1–3 (in the Atacama Desert, 18–26°S) with relatively high concentrations of metals, high abundance of quartz and low presence of arsenates, (ii) sites 4–8 (in northern Chile, 29–32°S) with relatively high abundance of quartz and low presence of metals and arsenates, (iii) sites 9–12 (in central Chile, 33–35°S) with anthropogenic enrichment of metals, relatively high values of quartz and low abundance of arsenates, (iv) sites 13–14 (also in central Chile, 35–37°S) with relatively high values of quartz and low presence of metals and arsenates, and v) sites 15–21 (in southern Chile, 37–41°S) with relatively high abundance of arsenates and low presence of metals and quartz. We found significant anthropogenic enrichment at sites close to Santiago (a major city of 6 million inhabitants) and in the Atacama Desert (that hosts several major copper mines).

Elemental and mineralogical composition of snow allows detecting deposition of pollutants and particulate matter<sup>1</sup>. Several studies have conducted chemical composition analysis of snow samples in Europe<sup>2–5</sup>, North America<sup>6,7</sup> and Asia<sup>8–11</sup>. However, efforts that have targeted the Andes<sup>12–14</sup> have been mostly conducted in snow on glacier surfaces at few points. Further analysis are needed, especially at snow-covered areas close to Santiago, Chile, a city of 6 million inhabitants (~33°S), with high levels of urban pollution and aerosols<sup>15,16</sup>.

Multiple climate regions can be identified along the Andes<sup>17–19</sup>. In our study area, the climate is modulated by the permanent influence of the South Pacific Anticyclonic (SPA) circulation that causes drier conditions in the Atacama Desert (18–32°S)<sup>20</sup>. The prevalent westerly circulation and the seasonal displacement of the SPA cause drier conditions in summer and wet conditions in winter in northern Chile (29–32°S), as well as in central Chile (33–37°S). Mountain snow precipitation associated with passing frontal systems (and cut-off lows) occurs mainly during the wet season (mid-April to September)<sup>20</sup>. Westerly circulation prevails in southern Chile (37–41°S) where frontal weather systems travel eastward generating snow precipitation as they cross the Andes<sup>21</sup>.

<sup>1</sup>Universidad de Santiago, Av. B. O'Higgins 3363, Santiago, Chile. <sup>2</sup>Instituto Venezolano de Investigaciones Científicas (IVIC), Apartado 20632, Caracas, 20632, Venezuela. <sup>3</sup>NorthWest Research Associates, Redmond, USA. <sup>4</sup>Department of Chemistry, University of Puget Sound, Tacoma, USA. <sup>5</sup>Unidad de Glaciología y Nieves, Ministerio de Obras Públicas, Santiago, Chile. <sup>6</sup>Centro GAIA Antártica, Universidad de Magallanes, Punta Arenas, Chile. <sup>7</sup>Centro de Estudios Avanzados en Zonas Áridas (CEAZA), La Serena, Chile. <sup>8</sup>Department of Physical Geography, Pontificia Universidad Católica de Chile, Santiago, Chile. <sup>9</sup>Center for Climate and Resilience Research, Universidad de Chile, Santiago, Chile. <sup>10</sup>Universidad Nacional Andrés Bello, Viña del Mar, Chile. <sup>11</sup>School of Earth, Energy and Environmental Sciences, Stanford University, Stanford, USA. <sup>12</sup>Center for Environmental Remote Sensing, Chiba University, Chiba, Japan. <sup>13</sup>Centro Mario Molina, Antonio Bellet 292, Santiago, Chile. <sup>14</sup>Harvard School of Public Health (HSPH), Boston, Massachusetts, USA. Correspondence and requests for materials should be addressed to R.R.C. (email: [raul.cordero@usach.cl](mailto:raul.cordero@usach.cl))

The snowpack is an important source of water for many Andean communities in central Chile (33–37°S), where also agriculture and power generation depend on the Andean streams<sup>22</sup>.

The snowpack in central and southern Chile (33–41°S) has been affected by mid-tropospheric warming<sup>23</sup> as well as by a persistent drought in 2010–2015<sup>24</sup> that has resulted in decreasing river flows<sup>25</sup>. In addition to anomalies in precipitation, the Andean snowpack (18–41°S) has been impacted by particulate matter transported by near-surface winds flowing from the valleys west of the Andes towards the mountains<sup>26,27</sup>. The prevailing circulation affecting the high Andean mountains is mainly westerly airflow, ranging from northwesterly to southwesterly direction<sup>21</sup>. The subsidence inversion (strengthened by the SPA and the local topography) confines the particles within the boundary layer in the Atacama Desert and central Chile. However, the same factors lead to near-surface local circulations (i.e. mountain-valley breeze), which enable particle transport/dispersion from sources (such as major mines) that operate over the Andes<sup>27</sup>.

Emissions from transport, industrial pollution and residential heating in Santiago (~33°S) have been found to affect the Andean snowpack<sup>14,26</sup>. However, the extent of anthropogenic enrichment in the Andean snowpack remains to be thoroughly tested. In the case of the Atacama Desert and central Chile, potential sources affecting the Andean snow include the mining industry<sup>13</sup>; Chile is the top producer of copper and molybdenum; it accounts for approximately one third of the global copper production while ranks third in molybdenum production<sup>28</sup>. In the case of southern Chile, impurities in the snow may result from wood stoves (the preferred heating system for the population in that area)<sup>29</sup> as well as from volcanic ash deposition<sup>30</sup>. Indeed, dozen of volcanoes are active in the Chilean Andes<sup>31,32</sup>. Because of the importance of the Andean snow for Chile, elemental and mineralogical composition analysis of the snowpack is a worthwhile effort.

In this paper, we report on the chemical composition analysis (major and trace elements, mineralogy, and chemical enrichment) of surface snow sampled during consecutive Austral winters (2015 and 2016) across a transect of about 2,500 km in the Chilean Andes (18–41°S). By combining the elemental and mineralogical composition of the snow samples, we were able to identify the five depositional environments shown in Fig. 1: (i) sites 1–3 (in the Atacama Desert) with relatively high presence of metals and quartz and low abundance of arsenates, (ii) sites 4–8 (in northern Chile,) with relatively high abundance of quartz and low presence of metals and arsenates, (iii) sites 9–12 (in central Chile) with anthropogenic enrichment of metals, relatively high values of quartz and low abundance of arsenates, (iv) sites 13–14 (also in central Chile) with relatively high values of quartz and low presence of metals and arsenates, and (v) sites 15–21 (in southern Chile) with relatively high abundance of arsenates and low presence of metals and quartz. As explained below, modest anthropogenic influence found in northern Chile and southern Chile suggests that element concentrations measured at sites in these zones may be useful as baselines for future studies.

## Material and Methods

**Sampling.** Sampling was conducted during consecutive Austral winters (2015 and 2016) at 21 sites across a transect in the Chilean Andes, from Putre to Volcán Osorno; see Table 1 and Fig. 1 for further details. Sampling was carried out at the end of the accumulation season. Sampling sites were selected to represent broad regions at locations with no known local aerosol sources. At each site, two samples from the surface layer (up to 15–20 cm depth) and separated by 1–2 m distance were collected. Samples ranged from 1 to 2 kg each.

Although some additional samples were collected from the subsurface layer, we focused on the surface layer since prior efforts have shown consolidation of pollutants in the surface layer with snowmelt<sup>33</sup>. Indeed, prior efforts at the same sampling sites allowed us to verify that subsurface layers tend to be cleaner than the surface<sup>26</sup>. Meteorological data suggest a lack of snowfall for at least five days before the sampling at most sampling sites. At sites 3 and 4, cold fronts brought snowfall to the area immediately prior to sampling. Although in these cases the surface layer was cleaner than the subsurface layer, element concentrations were found to be comparable (of the same order).

Researches conducting sampling in the field took care to prevent sample contamination. As also explained by Rowe *et al.*<sup>26</sup>, a stainless steel spatula was used and samples were placed into plastic bags, in turn packed in Whirlpack bags. Styrofoam coolers were used for transportation to the laboratory. In the laboratory deionised water was used for washing tools and containers before filtering, while latex gloves and lab coats were worn during filtering. Snow samples were transferred to a glass beaker and snowmelt was thereafter vacuum-filtered, leaving the insoluble material on the filter. Stainless-steel funnels and 0.4- $\mu$ m Nucleopore filters were used. Filters were afterwards placed in sterile petri dishes.

**Chemical composition.** Elemental composition of the insoluble material in the snow samples was carried out using Energy dispersive X-ray fluorescence (EDXRF) spectrometry. EDXRF is a technique widely used for elemental analysis of particles on filter media<sup>34,35</sup>. Elemental analysis was conducted at the Harvard School of Public Health (HSPH) using an Epsilon 5 EDXRF spectrometer (PANalytical, The Netherlands). The procedure at HSPH for analysing elements on filters is described by Kang *et al.*<sup>35</sup>; it involves using 49 MicroMatter XRF calibration standard polycarbonate films (Micromatter Co., Vancouver, Canada) spanning from Na (atomic number 11) to Pb (atomic number 82). When intercomparing measurements of standard films, the HSPH EDXRF spectrometer has exhibited good performance: “2% errors in precision (suggesting a good reproducibility) and 4% errors in accuracy (showing a proper calibration)”<sup>35</sup>. In the case of the lower concentrations associated with field samples, the HSPH EDXRF spectrometer has exhibited a reproducibility within 15% for most of the elements<sup>35</sup>. For this study, concentrations of Al, Mg, Si, P, Ca, Ti, S, K, V, Cr, Mn, Ni, Cu, Fe, Co, Zn, Rb, Sr, Zr, Mo, Ba and Pb were determined to be significant.

Mineralogy was assessed using X-ray powder diffraction (XRD)<sup>36</sup>. A Siemens D-5005 x-ray diffractometer fitted with parallel beam geometry and Cu K $\alpha$  radiation, was applied. XRD patterns were collected every 0.02°,

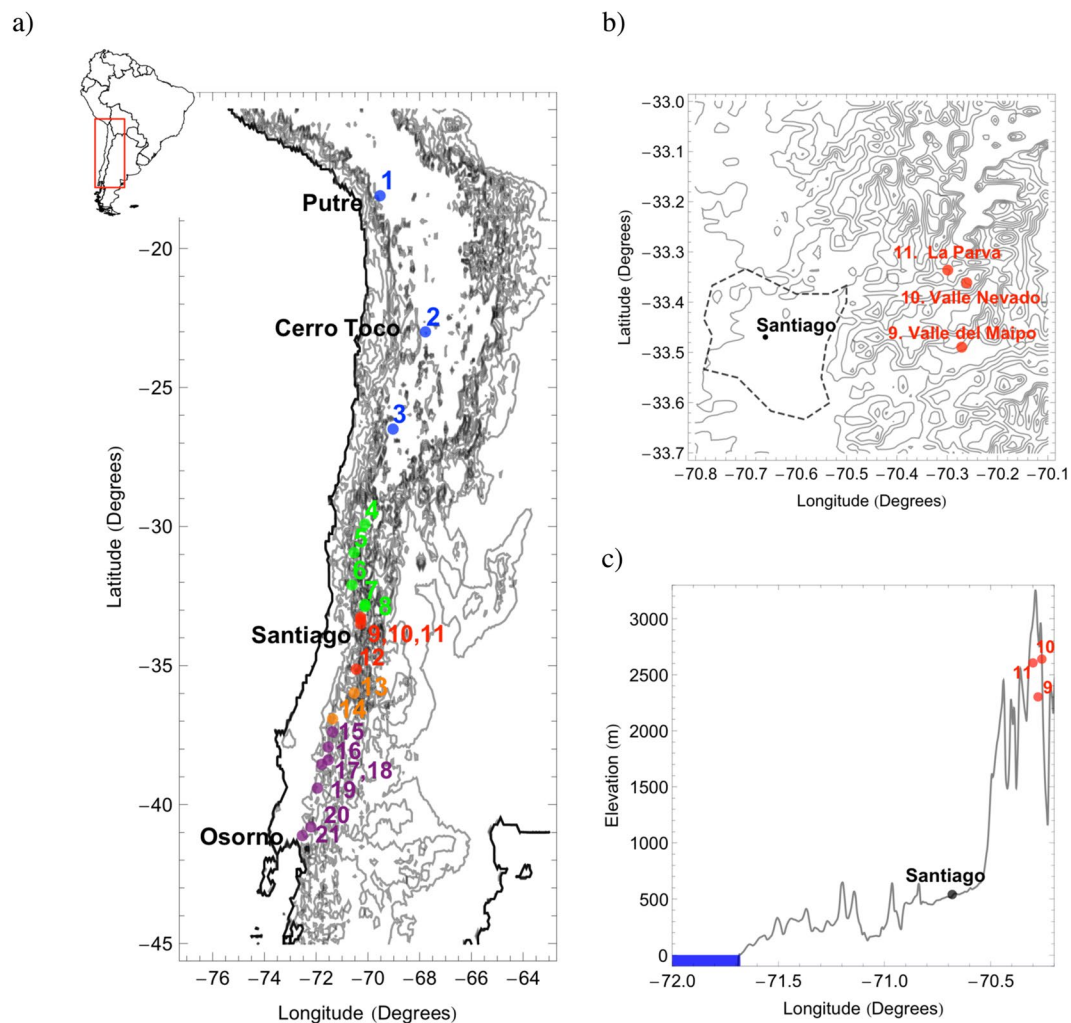


**Figure 1.** (a) Sampling Sites. Numbers identify the 21 sampling sites indicated in Table 1. Color code indicates the five different depositional environments identified in this study. (b) Sampling sites 9–11 nearby Santiago ( $33^{\circ}27'S$ ;  $-70^{\circ}41'W$ ); dotted line indicates the metropolitan area of this major city. (c) Elevation along latitude  $33^{\circ}27'S$ . Plots generated by using PYTHON's Matplotlib Library (<https://matplotlib.org>)<sup>62</sup>.

from  $5^{\circ}$  to  $90^{\circ}$ . Minerals were identified at the Instituto Venezolano de Investigaciones Científicas (IVIC) from their characteristic peaks.

**Statistical analysis.** Cluster analysis and principal components analysis (PCA) were used to assess element assemblages. Before applying the multivariate statistical analysis, concentrations rendered by EDXRF were log-transformed and standardized (by subtracting the mean and dividing the outcome by the standard deviation)<sup>37</sup>. An orthogonal method (the varimax method) was applied for factor rotation<sup>37</sup>. We evaluated the following cluster analysis methods: Ward, complete linkage, single linkage, weighted pair-group average, unweighted pair-group average and unweighted pair-group centroid. STATISTICA<sup>38</sup> was used to conduct the calculations.

In order to detect relative contributions of anthropogenic sources, we applied Crustal enrichment factors ( $EF_{UCC}$ )<sup>5,39–41</sup>.  $EF_{UCC}$  was taken as the ratio between the concentration of an element and the concentration an element originated from rocks and/or dust. As pointed out by Cantonati *et al.*<sup>41</sup> and Veyseyre *et al.*<sup>42</sup>, enrichment factors within the range 0.1–10 allow discarding the significant presence of elements other than those from rocks and dust, while  $EF_{UCC}$  values higher than 10 do suggest contributions from different sources (natural and/or anthropogenic);  $EF_{UCC}$  values within the range 10–500 (moderate enrichment) indicate input sources additional to crustal material, while  $EF_{UCC}$  values higher than 500 (high enrichment) suggest pronounced anthropogenic contribution<sup>41,42</sup>. In this study,  $EF_{UCC}$  values were calculated for each sampling site. In addition, a second technique for estimating metal enrichments was applied. It implied normalizing the metal concentrations against an element of detrital origin<sup>43</sup>. Following prior efforts<sup>44–46</sup>, we normalized the element concentrations against Al.

**Back-trajectory computation.** Air-parcel backward trajectories were applied to sampling sites where we found anthropogenic enrichment. We used the Hybrid Single-Particle Lagrangian Integrated Trajectory (HYSPPLIT) model<sup>47–49</sup> fed with the Global Data Assimilation System (GDAS) archive (available in a resolution of three hours and a  $1^{\circ}$  latitude-longitude)<sup>50</sup>. At each site we computed 36-h backward trajectories by using

Sites	Location	Latitude	Longitude	Elevation (m)	Sampling date
1	Putre	S 18°06'08.5"	W 69° 31'14.3"	5318	2015/07/05
2	Cerro Toco	S 22°57'09.4"	W 67°46'38.1"	5370	2015/07/10
3	La Ola	S 26°27'17.1"	W 69°03'0.72"	3578	2015/07/14
4	Valle del Elqui	S 29°20'42.6"	W 70°04'17.9"	2341	2015/07/17
5	La Ramada	S 30°57'38.1"	W 70°33'21.2"	1757	2015/07/19
6	Valle Choapa	S 32°03'49.2"	W 70°35'42.4"	1919	2015/07/20
7	Portillo	S 32°50'1.4"	W 70°7'59.2"	2800	2015/07/21
8	Los Hornos	S 32°53'32.2"	W 70°12'64.1"	2322	2015/07/22
9	Valle de Maipo	S 33°29'45.8"	W 70°16'35.5"	2302	2015/07/26
10	Valle Nevado	S 33°21'58.3"	W 70°15'16.3"	2635	2015/07/24
11	La Parva	S 33°20'06"	W 70°18'00.7"	2610	2016/07/25
12	Curicó	S 35°08'10.8"	W 70°28'45.2"	1860	2016/08/19
13	Maule	S 35°59'19.7"	W 70°33'45.1"	1860	2016/08/20
14	Chillán	S 36°54'26.4"	W 71°23'59.5"	1963	2016/07/23
15	Antuco	S 37°22'04.6"	W 71°22'57.3"	1494	2016/08/23
16	Volcán Collaqui	S 37°52'35.1"	W 71°28'26.9"	1142	2016/08/24
17	Corralco	S 38°24'21.1"	W 71°33'34.3"	1601	2016/08/27
18	Volcán Llaima	S 38°31'37.8"	W 71°47'44.5"	1830	2016/08/28
19	Volcán Villarrica	S 39°23'46.9"	W 71°57'53.0"	1450	2016/08/29
20	Antillanca	S 40°47'12.5"	W 72°11'31.5"	1349	2016/07/19
21	Volcán Osorno	S 41°07'12.0"	W 72°31'47.7"	1326	2016/08/31

**Table 1.** Sampling sites.

meteorological data over a 92-day period prior to the sampling date (see Table 1). Over that period, trajectories were computed every 3 hours, making a total of 736 trajectories per site. These trajectories were divided into clusters following a cluster analysis based on the total spatial variance (TSV)<sup>51</sup>.

## Results

**Chemical composition.** Figure 2 shows the boxplots of the element concentrations (ng of the element per g of snow) in the snow samples collected in the five depositional environments indicated in Fig. 1. As shown in Fig. 2, for all sets, either Si or Fe exhibited the highest concentration followed in general by K or Ca, Al, Ti and Mg. Figure 2 also allows realizing the dispersion of element concentrations found in Andean snow (18–41°S). It can be observed that the concentrations of Co, Cu, Rb, Ba and V ranged within three orders of magnitude. Concentrations of Mg, P, K, Ni, Zn, Sr, Zr, Ti, Mn, Mo, Pb and Fe ranged within two orders of magnitude, while the other elements ranged only within one order of magnitude.

Table 2 shows the best estimates of the element concentrations (ng of element per g of snow) in the snow samples at each site while the associated uncertainty are shown in Table 3. We found relatively high concentrations of K, Ti, V, Mn, Fe, Co, Zn, Rb, Sr, Ni, Cu, Zr, Mo, Ba and Pb at site 11 (La Parva, nearby Santiago), while at site 2 (Cerro Toco, in the Atacama Desert) relatively high concentrations of Al and Si were detected.

We found relatively high concentrations of Mg and Ca at site 3 (La Ola, in northern Chile), whereas at site 10 (Valle Nevado, also near Santiago), 14 (Chillán, in central Chile) and 19 (Volcán Villarrica, in southern Chile), relatively high concentrations of Cr, S and P, were measured, respectively.

The lowest concentrations of Si, K, Ti, Fe, Co, Ni, Cu, Zn, Sr, Zr and Ba were found at site 20 (Antillanca, in southern Chile), while at site 19 (Volcán Villarrica, also in southern Chile) we detected the lowest concentrations of V, Rb and Pb.

The lowest concentrations of Al and Mo were measured at site 15 (Antuco, central Chile), while at sites 2 (Cerro Toco, in the Atacama Desert), 6 (Valle Choapa, in northern Chile), 8 (los Hornos, in northern Chile), 13 (Maule, in central Chile), 16 (Volcán Collaqui, in southern Chile) and 21 (Volcán Osorno, also in southern Chile), we found the lowest concentrations of P, Ca, Cr, Mg, Mn and S, respectively. See Table 2 for further details.

**Statistical analysis.** Cluster analysis and PCA were carried out on the dataset in Table 2 (after normalization and standardization). Table S1 shows the correlation matrix for the element concentrations.

Figure 3 shows the dendrogram obtained from the cluster analysis (of elemental concentrations) using the unweighted pair-group average method. Two groups are identified: (i) group 1 consists of sites 1–3 (in the northern Atacama Desert, 18–26°S), sites 9–11 (relatively close to Santiago, ~33°S) and site 12 (close to Curicó, ~35°S); (ii) group 2 consists of sites 4–8 (in northern Chile, 29–32°S), sites 13–14 (in central Chile, 35–37°S), and sites 15–21 (in southern Chile, 37–41°S). Dendrograms from the cluster analysis for other linkage methods (the single linkage method, complete linkage method, unweighted pair-group centroid method, Ward's method, and weighted pair-group average method) consistently suggest the same two groups shown in Fig. 3.

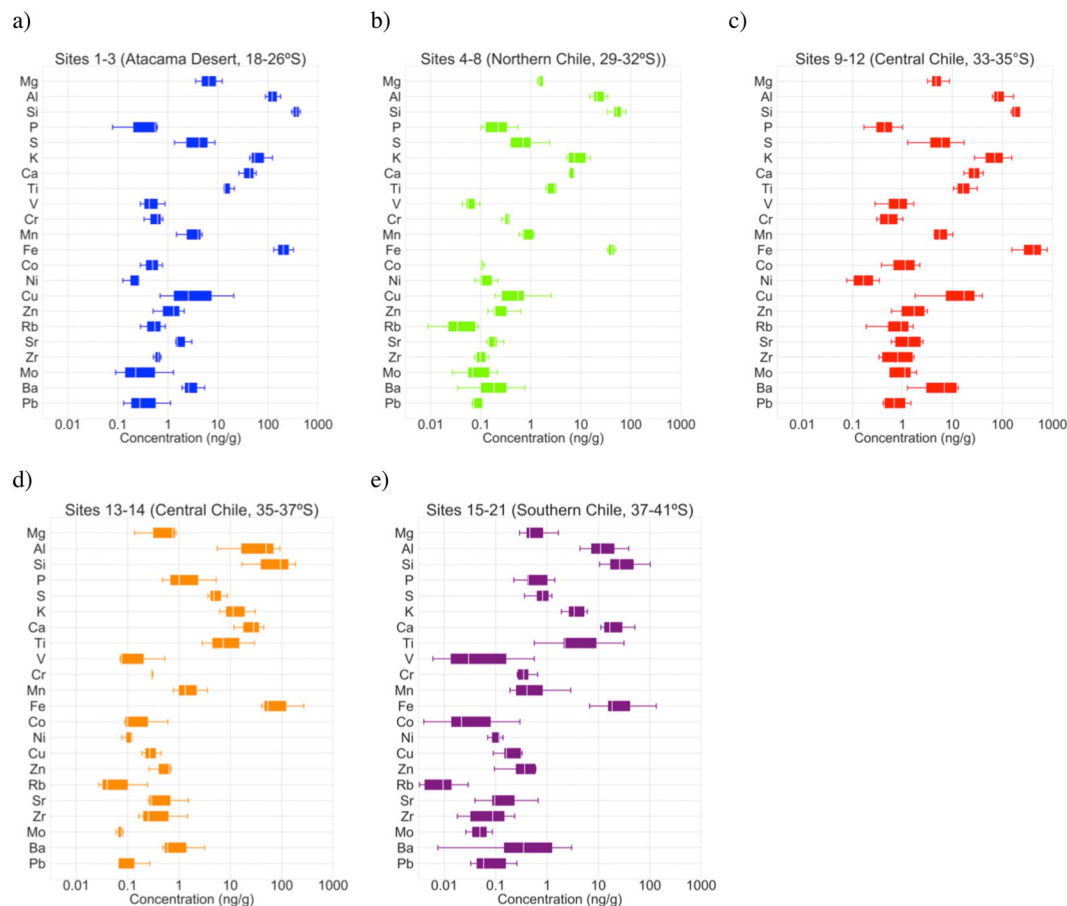


**Figure 2.** Element concentrations (ng of the element per g of snow) in the snow samples collected in: (a) sites 1–3 (in the Atacama Desert); (b) sites 4–8 (in northern Chile); (c) site 9–12 (in central Chile); (d) sites 13 and 14 (also in central Chile); and (e) sites 15–21 (in southern Chile). In each box, the central mark (white stripe) indicates the median, and the edges indicate the 25th and 75th percentiles. The whiskers extend to the most extreme data points. Plots generated by using PYTHON's Matplotlib Library (<https://matplotlib.org>)<sup>62</sup>.

PCA results are shown in Table 4, while Fig. 4 shows scores and loading. Two principal components accounted for 81% of the total variance. Component 1 (eigenvalue equal to 16.1) presented significant negative loads of Mg, Al, Si, S, K, Ti, V, Cr, Mn, Fe, Co, Ni, Cu, Zn, Rb, Sr, Zr, Mo, Ba and Pb. Component 2 (eigenvalue equal to 1.7) has a high positive load of P. The PCA results (see Fig. 4b) also distinguished the same two groups suggested by the cluster analysis.

**Mineralogy.** Table 5 shows the bulk mineralogy of the snow samples, as the percentage of each mineral in the insoluble material filtered from snow. The main mineralogical species were: silicates (labradorite, microcline, albite), hydrated silicates (muscovite, laumontite, K-Fe-Mg-Al hydroxysilicate, biotite), quartz, hydrated sulphates, oxides, hydrated oxides, as well as hydrated arsenates at sites 15–21 (in southern Chile).

**Enrichment factors.** Table 6 shows the enrichment factors ( $EF_{UCC}$ ) of elements found in the snow. Mg, Si, P, S, K, Ca, Ti, Sr and Zr showed no significant enrichment ( $EF_{UCC} < 10$ ) in the snow samples. In the case of V, Cr, Mn, Fe, Co, Ni, Zn, Rb, Ba and Pb,  $EF_{UCC}$  distributions ranged from no enrichment at some sites to moderate enrichment ( $10 < EF_{UCC} < 500$ ) at others. Cu and Mo presented in general relatively high enrichments, from moderate ( $10 < EF_{UCC} < 500$ ) to intense ( $EF_{UCC} > 500$ ). Our results show a high enrichment of Cu at site 2 (Cerro Toco, in the Atacama Desert) and both Cu and Mo at sites 9–11 (close to Santiago).

Figures S1–S5 show the correlation between Al concentration and the concentration of Ti, V, Cr, Mn, Fe, Co, Ni, Cu, Zn, Rb, Sr, Zr, Mo, Ba and Pb. The dashed lines in Figs S1–S5 represent 95% confidence interval. Values found well above these lines represent metals enrichment at a particular site. Again, our results indicate enrichment of Ni, Mn, Ti, V, Co, Cu, Zn, Zr, Ba and Pb at site 10 (Valle Nevado) and at site 11 (La Parva); of Fe, Rb and Mo at sites 9–11 (Valle de Maipo, Valle Nevado, and La Parva); and of Sr and Cr at site 10 (Valle Nevado). These results are consistent with significant enrichments previously reported<sup>14</sup> in the case of snow sampled at Cerro Colorado (in the very same area of our sampling sites 10 and 11). The correlations in Figs S1–S5 also suggest enrichments of Cr and Ni at site 1 (Putre in the Atacama Desert), and of Mn at site 12 (close to Curicó).



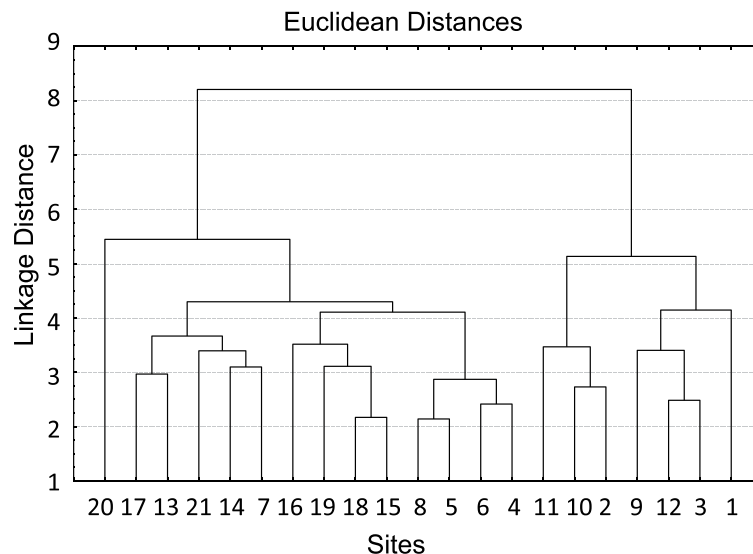


**Figure 3.** Dendrogram obtained from the cluster analysis of elemental concentrations using the unweighted pair-group average method. Numbers in the horizontal axis identify the 21 sampling sites indicated in Table 1. Plot generated by using STATISTICA (data analysis software system, version 7, <http://www.statsoft.com/Products/STATISTICA-Features>)<sup>38</sup>.

Element	Factor 1 (73%)	Factor 2 (8%)
Mg	−0.78157	−0.410716
Al	−0.88805	0.064792
Si	−0.90495	−0.069823
P	0.11635	<b>0.906353</b>
S	−0.76154	0.088118
K	−0.97397	−0.132094
Ca	−0.56330	0.651318
Ti	−0.95559	0.045982
V	−0.93353	−0.047603
Cr	−0.76222	−0.025786
Mn	−0.92033	0.080591
Fe	−0.97410	−0.074116
Co	−0.92930	0.014289
Ni	−0.76986	−0.044991
Cu	−0.88857	−0.179315
Zn	−0.84932	0.285502
Rb	−0.92863	−0.156184
Sr	−0.96084	0.103885
Zr	−0.92083	0.126097
Mo	−0.86036	−0.141991
Ba	−0.85242	0.220138
Pb	−0.88566	−0.060095

**Table 4.** Principal factors obtained after a varimax rotation. The percentages of each factor are shown in parentheses. Two factors explain 81% of the total variance.

(see details below), the metal concentrations found in snow samples of group 2 are comparable to metal concentrations (attributed to deposition of background atmospheric aerosols) previously reported for snow samples collected in remote areas in Europe (Eastern Alps<sup>2</sup>, Central Pyrenees<sup>5</sup>, and French Alps<sup>42</sup>), and North America (Alaska<sup>6</sup>).

The two principal components (that explained 81% of the total variance in the PCA) suggest the origin of the elements in each group. Component 1 is characterized by high negative loads of Mg, Al, Si, S, K, Ti, V, Cr, Mn, Fe, Co, Ni, Cu, Zn, Rb, Sr, Zr, Mo, Ba and Pb, while Component 2 exhibits a high positive load of P. Component 1 includes elements that are abundant in the crust (Al, Ti, Mn and Fe), which pointed at terrigenous dust deposition<sup>5</sup>. Moreover, Component 2 includes P, often used in herbicides and pesticides. The position of sites 13 (Maule)

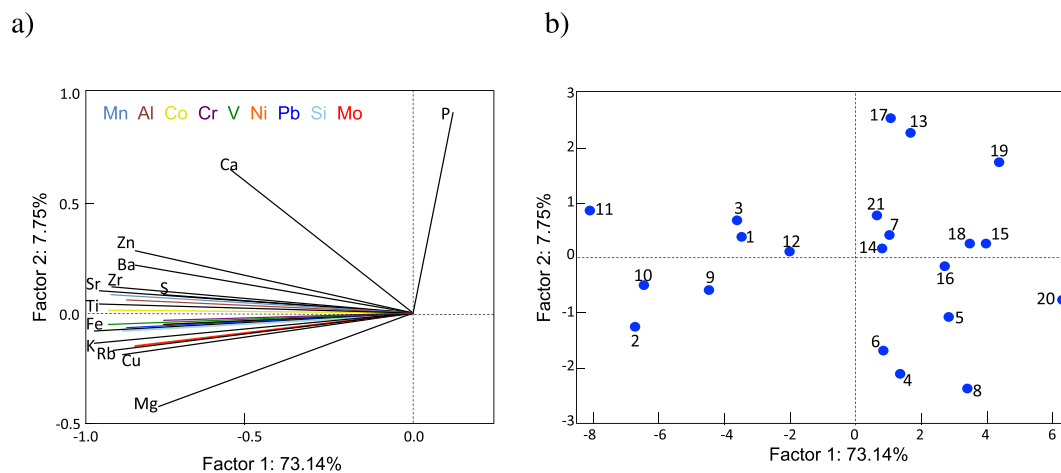


**Figure 4.** Principal component analysis (PCA). Plots generated by using STATISTICA (data analysis software system, version 7, <http://www.statsoft.com/Products/STATISTICA-Features>)<sup>38</sup>. (a) Projections of elements on the factor-plane. (b) Projections of sites on the factor-plane; numbers identify the 21 sampling sites indicated in Table 1.

Site	qz	sil	h.sil	oxi	h.oxi	h.sulp	h.pho	fluo	h.arse	carb	h.carb	rar.er	unin.ph
1	***	*****	*****	**		***							
2	****	*****	***	***		*							
3	***	*****	***	***		***							
4	**	***	*****	**		***	***						
5	***	*****	***	*		***	**						
6	**	***	*****	***		***							
7	***	*****	***	***		*							
8	***	*****	***	*	**	***							
9	**	***	*****	*	*	**							
10	***		***	**	*	*****							
11	*****	*	***	**	*	***	***						
12	****	*	*****	**			**	***					
13	***	***	***		***	***							
14	***	*****	*****	**		*	**				*		
15		*****				***			*****				
16		*****	***	**			***		**				
17			***	**	***		***		*****			**	
18		****	***						***		***		
19			*****	**	***	***		**	***				
20		*****	**			***			***	***	***		
21		*****	**			***			***			**	**

**Table 5.** Bulk mineralogy of the snow samples. qz: quartz, sil: silicates, h.sil: hydrated silicates, oxi: oxides, h.oxi: hydrated oxides, h.sulp: hydrated sulphates, h.pho: hydrated phosphates, fluo: fluorides, h.arse: hydrated arsenates, carb: carbonates, h.carb: hydrated carbonates, rar.er: rare earth, and unin.ph: unidentified phases. \* < 5%, \*\* (5–10)%, \*\*\* (11–20)%, \*\*\*\* (21–30)%, \*\*\*\*\* (31–40)%, > 40%.

and 17 (Corralco) in Fig. 4b highlights the loading of P in snow samples at these sites. However, the low crustal enrichment factor for P (see Table 6) does not support significant effects of the agricultural activity on the snow-pack in the area of Maule and Corralco.

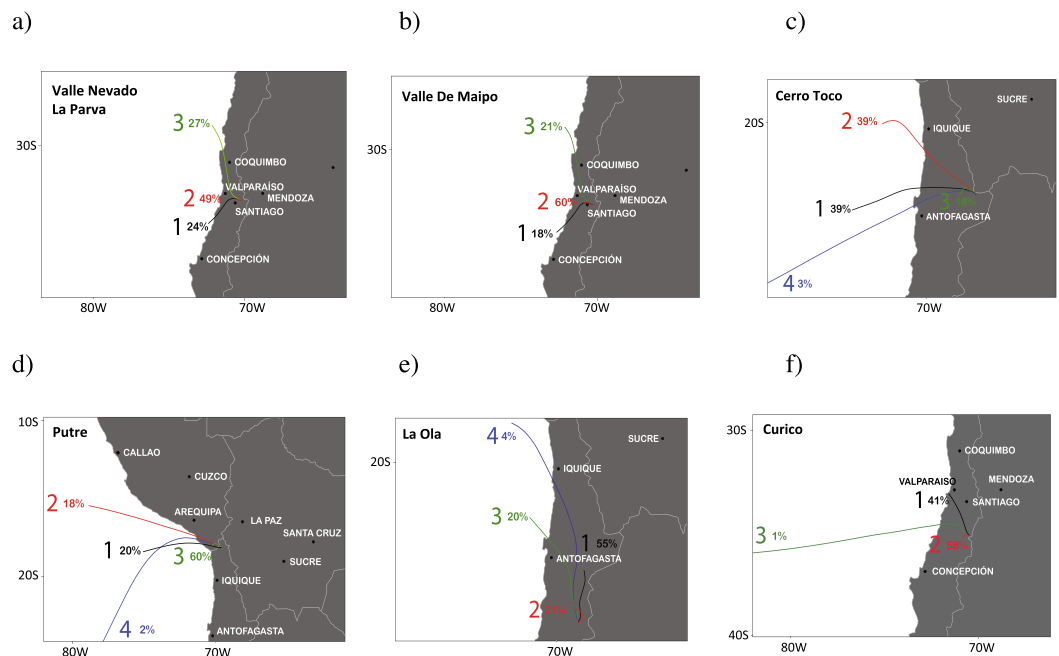
In all of the samples, Cu and Mo exhibited the highest enrichment factors ( $EF_{UCC}$ ), from moderate to intense. Element concentrations of both Cu and Mo show a very good correlation (Pearson coefficient = 0.98, see Table S1), which suggests that they have a common origin. This result is consistent with the fact that concentrations of hypogene Cu (0.40–0.86%) and Mo (0.01–0.025%) have been reported for the Andes in 18 major deposits (in Chile, Argentina and southern Peru)<sup>52</sup>. Chile is currently the top producer of copper (accounting for about one third of the global copper production) and ranked third in molybdenum production<sup>28</sup>.

Figure 5 shows the 36-h back trajectory clusters for sites where we found significant anthropogenic enrichment. Back trajectories were computed every 3 hours using meteorological data over a 92-day period prior to the



Sites	Mg	Si	P	S	K	Ca	Ti	V	Cr	Mn	Fe	Co	Ni	Cu	Zn	Rb	Sr	Zr	Mo	Ba	Pb
1	0.2	1	1	3	1	1	3	3	14	2	3	15	9	31	6	2	3	1	103	2	5
2	0.2	1	0.1	4	2	1	3	7	8	4	5	29	6	627	18	3	4	1	399	4	29
3	0.5	1	1	1	1	2	4	7	8	7	6	37	6	157	22	4	4	2	56	2	14
4	1	1	0.4	2	1	1	2	3	20	5	4	20	13	31	8	2	1	1	92	1	14
5	0.5	1	2	2	1	1	3	4	41	5	5	39	22	78	15	1	2	1	80	1	18
6	0.3	1	1	7	1	1	3	5	26	3	4	28	15	493	17	2	2	1	421	1	11
7	0.4	1	3	3	1	3	4	3	39	8	5	34	24	186	45	1	2	2	387	4	23
8	0.5	1	1	2	1	1	3	5	39	7	6	29	21	201	14	0.4	2	2	253	0.3	22
9	0.3	1	0.5	6	3	0	4	11	10	7	9	61	6	734	19	6	2	2	596	5	23
10	0.3	1	0.3	7	2	1	7	25	36	16	21	168	15	2055	61	13	8	8	1141	21	74
11	0.3	1	1	3	2	1	5	15	9	9	12	89	9	1287	28	7	4	3	636	9	40
12	0.3	1	1	1	1	1	4	6	9	9	5	35	4	135	12	2	2	2	86	2	26
13	0.1	0.2	6	12	1	3	3	4	27	8	4	23	13	57	38	1	2	2	165	3	12
14	0.1	0.5	1	8	1	1	4	2	13	2	3	13	10	21	8	0.4	1	2	66	1	6
15	0.2	1	8	6	1	3	5	4	72	6	4	22	42	161	49	1	2	3	132	0.2	24
16	0.2	0.2	2	4	0.4	1	3	9	28	1	2	5	16	190	20	0.1	1	0.2	95	7	26
17	0.1	1	4	2	0.4	3	1	5	15	6	2	51	7	39	23	0.3	4	2	50	2	21
18	0.4	1	5	6	1	4	5	3	56	5	4	13	40	79	76	0.2	2	3	249	1	56
19	0.1	0.2	6	4	0.3	2	2	0.3	29	2	1	2	18	30	21	0.1	1	0.5	180	1	6
20	0.1	0.1	1	2	0.2	2	1	0.5	24	1	1	1	13	20	6	0.2	0.4	0.4	112	0.2	9
21	0.3	1	1	1	0.5	3	5	7	24	6	5	31	11	23	7	1	3	2	56	10	5

**Table 6.** Crustal enrichment factor ( $EF_{UCC}$ ).



**Figure 5.** 36-h back trajectory clusters. (a) Valle Nevado/La Parva; (b) Valle del Maipo; (c) Cerro Toco; (d) Putre; (e) La Ola; (f) Curicó. Plots generated by the using MeteoInfo software tools for meteorological data visualization<sup>63</sup>.

sampling date making a total of 736 trajectories for each site. Back trajectories from sites 9–12 were divided into 3 clusters, while trajectories from sites 1–3 were divided into 4 clusters.

Figure 5a,b show the back trajectory clusters for sites 9–11, which are situated less than 20 km east of heavily populated urban areas of Santiago (clusters for Valle Nevado and La Parva are shown in a single plot since these sites are very close each other). Cluster 2 was the largest in Fig. 5a,b. This cluster suggests a heavy influence from Santiago, as a majority of the trajectories (49% in Fig. 5a and 60% in Fig. 5b) originated in or passed over Santiago, and are characterized by being short, with low wind speeds. The second most frequent cluster in Fig. 5a (Fig. 5b) was number three, which contained 27% (21%) of all trajectories. These trajectories typically indicated a source

area in northern Chile but passing close to Los Bronces (a major copper mine). Sites 9 (Valle del Maipo), 10 (Valle Nevado) and 11 (La Parva) are located about 30 km south in the case of site 9 (and about 15 km south in the case of sites 10 and 11) of Los Bronces. Cu and Mo exhibited high enrichment factors ( $EF_{UCC} > 500$ ) at sites 9–11.

Cu also exhibited a high enrichment factor ( $EF_{UCC} > 500$ ) at site 2 (Cerro Toco). This site is located in the Atacama Desert, a region whose main economic activity is the copper mining industry. Figure 5c shows that Cluster 2 contained 39% of the trajectories for Cerro Toco. This cluster represented air coming out of the northwest passing close to several major copper mines (Radomiro Tomic, Ministro Hales and Chuquicamata, the latter being one of the largest copper mines in the world). Cerro Toco is located within 150 km of these major copper mines. Cluster 1 also contained 39% of all trajectories for Cerro Toco. These trajectories typically indicated a source area west of Cerro Toco and pass over important astronomical projects (powered by diesel generators) located only few km west of the sampling site.

Figure 5d,e shows the back trajectory clusters for site 1 (Putre) and site 3 (La Ola). Cluster 3 in Fig. 5d, containing 60% of all trajectories, was the largest. The routes for this cluster were typically short and indicated a slow wind speed. The majority of these trajectories originated in the area close to Tacna (a Peruvian city of about 300,000 inhabitants) and to a major gold mine (Pucamarca) in the Peruvian side of the border. Site 1 is located about 70 km east of Tacna and about 40 km southeast of the Pucamarca mine. In the case of site 3 (La Ola), Fig. 5e shows that Cluster 1 contained 55% of the trajectories. This cluster represented air coming out of the north. Some trajectories in this cluster originated from nearby a major copper mine (La Escondida), located about 220 km north of the sampling site. The second most frequent cluster in the case of La Ola was number two, which contained 21% of all trajectories. These trajectories typically indicated a source area about 60 km northwest of the sampling site, close to another major copper mine (El Salvador).

Figure 5f shows the clusters for site 12 (Curicó). Cluster 2 was the largest of the 3, containing 58% of the back trajectories. These trajectories were typically characterized by slow air movement, with the trajectories extending about 60 km from the west to the receptor site. Cluster 1 was the second most common path. This cluster contained 41% of the total trajectories. These trajectories were faster and pass over the most populated and industrialized areas in Chile. Still, due to the moderate  $EF_{UCC}$  values, an anthropogenic influence can be considered modest at site 12.

**Volcanic activity.** There are more than one hundred volcanoes in the Chilean Andes that have been active during the Holocene<sup>31</sup>. Several of these volcanoes are currently active<sup>32</sup>. Areas surrounding active volcanoes are subjected to volcanic ash deposition<sup>30</sup>. In active geothermal systems in the southern Andes of Chile, As is present in borehole fluids<sup>53</sup>. In thermal waters in the southern volcanic zone (SVZ), As is transported from geothermal reservoirs to the surface<sup>54</sup>. In eruptive gases, arsenic predominates in the form of  $As(OH)_3$ <sup>55</sup>. Ash can absorb  $As(OH)_3$  (as well as similar to volatile compounds)<sup>56</sup>. A part of the magmatic arsenic could also be incorporated into the glass structure<sup>57,58</sup>. As discussed by Bia *et al.*<sup>58</sup>, partial remobilization of structural As can occur when dissolution of aluminosilicate glass dissolute, which is favored by extreme acid conditions; volatile acids (such as HCl,  $H_2S$ , and HF) in the volcanic plume can produce such conditions<sup>58</sup>.

Silicates (quartz, silicates and hydrated silicates in Table 5) were found to be the dominant minerals at every sampling site. However, the volcanic activity fingerprint on the snow was apparent in samples taken in southern Chile. Our results indicate that sites 15–21 have relatively low quartz concentration and high concentrations of arsenates. These sites are located in the very active SVZ, where prior studies have shown absence<sup>59</sup> or minor amount<sup>60</sup> of quartz in ashes. The predominant minerals detected in fault-controlled hydrothermal systems in the southern Andes are Ca and Ca (-Na) zeolites, minor quartz was also locally found<sup>61</sup>. The relatively low quartz concentration at sites 15–21 suggests a reduction of amorphous silica by carbon monoxide during the frequent explosive eruptions in the zone.

## Summary and Conclusions

We have carried out a chemical composition analysis (major and trace elements, mineralogy, and chemical enrichment) of surface snow sampled across a transect of about 2,500 km in the Chilean Andes (18–41°S).

Cluster analysis and principal component analysis (PCA) applied to the element concentration data, rendered consistent figures suggesting two main groups: (i) group 1 consists of sites 1–3 (in the Atacama Desert, 18–26°S), sites 9–11 (close to Santiago, ~33°S) and site 12 (close to Curicó, ~35°S); (ii) group 2 consists of sites 4–8 (in northern Chile, 29–32°S), sites 13–14 (in central Chile, 35–37°S), and sites 15–21 (in southern Chile, 37–41°S).

Group 1 exhibited significantly higher concentrations of several metals (Al, Si, Ti, Cr, Fe, Co, Ni, Cu, Zn, and Pb) than group 2. Indeed, with the exception of Cu and Mo, metal concentrations found in snow samples of group 2 are comparable to metal concentrations (attributed to the deposition of background atmospheric aerosols) previously reported for snow samples collected in remote areas elsewhere.

Cu and Mo exhibited the highest enrichment factors (moderate-intense) in all samples. The very good correlation between concentrations of both Cu and Mo is consistent with the fact that major mineral deposits in the Andes contain both elements.

Our results confirm significant anthropogenic enrichment (Cu and Mo) at sites near Santiago (sites 9–11). These sites are located about 30 km south in the case of site 9 (and about 15 km south in the case of sites 10 and 11) of Los Bronces, a major copper mine. Anthropogenic enrichment (Cu) was also found at Cerro Toco in the Atacama Desert (site 2), located within 150 km of several major copper mines (Radomiro Tomic, Ministro Hales and Chuquicamata).

Moreover, our results confirm the influence of Santiago (a major city of 6 million inhabitants) on the snow-pack nearby. We found significant enrichment of Ni, Mn, Ti, V, Co, Cu, Zn, Zr, Ba and Pb at site 10 (Valle Nevado) and at site 11 (La Parva); of Fe, Rb and Mo at sites 9–11 (Valle de Maipo, Valle Nevado, and La Parva); and of Sr and Cr at site 10 (Valle Nevado). These results were expected since these sites are located less than 20 km east of heavily populated urban areas of Santiago.

We have also detected the fingerprint of volcanic ash deposition on snow samples taken in southern Chile (37–41°S), an area with a dozen of active volcanoes. Our results at sites 15–21 exhibited a relatively low quartz concentration and high concentrations of arsenates, which is consistent with prior studies that showed the absence or minor amounts of quartz in ashes.

Our elemental and mineralogical analysis allowed us to identify five depositional environments: (i) sites 1–3 (in the Atacama Desert, 18–26°S) with relatively high concentrations of metals, high abundance of quartz and low presence of arsenates, (ii) sites 4–8 (in northern Chile, 29–32°S) with relatively high abundance of quartz and low presence of metals and arsenates, (iii) sites 9–12 (in central Chile, 33–35°S) with anthropogenic enrichment of metals, relatively high abundance of quartz and low presence of arsenates, (iv) sites 13–14 (also in central Chile, 35–37°S) with relatively high values of quartz and low abundance of metals and arsenates, and (v) sites 15–21 (in southern Chile, 37–41°S) with relatively high presence of arsenates and low abundance of metals and quartz.

Our results have important implications for many Andean communities, especially in central Chile (33–37°S), where we found significant anthropogenic enrichment. In this region the snowpack is important for urban water supply, power generation, and agriculture<sup>22</sup>. Moreover, our findings are consistent with prior efforts<sup>26</sup> that have shown that presence of higher concentrations of light-absorbing impurities in the Andean snow in the Atacama Desert and at locations nearby Santiago.

## Data Availability

The datasets generated and analyzed during the current study are available from the corresponding author on reasonable request. For the trajectory analysis, we used the Global Data Assimilation System (GDAS1) Archive Information provided through the Real-time Environmental Applications and Display sYstem (READY) (<http://ready.arl.noaa.gov/gdas1.php>).

## References

- Telmer, K., Bonham-Carter, G. F., Kliza, D. A. & Hall, G. E. M. The atmospheric transport and deposition of smelter emissions: evidence from the multi-element geochemistry of snow, Quebec, Canada. *Geochim. Cosmochim. Acta* **68**, 2961–2980 (2004).
- Gabrielli, P., Cozzi, G., Torcini, S., Cescon, P. & Barbante, C. Trace elements in winter snow of the Dolomites (Italy): A statistical study of natural and anthropogenic contributions. *Chemosphere* **72**, 1504–1509 (2008).
- Pilecka, J., Grinfeld, I., Valujeva, K., Straupe, I. & Purmalis, O. Heavy metal contamination and distribution in the urban environment of Jelgava. *J. Environ. Eng. Landsc.* **1**, 173–179 (2017).
- Siudek, P., Frankowski, M. & Siepak, J. Trace element distribution in the snow cover from an urban area in central Poland. *Environ. Monit. Assess.* **187**, 225–240 (2015).
- Bacardit, M. & Camarero, L. Atmospherically deposited major and trace elements in the winter snowpack along a gradient of altitude in the Central Pyrenees: The seasonal record of long-range fluxes over SW Europe. *Atmos. Environ.* **44**, 582–595 (2010).
- Douglas, T. A. & Sturm, M. Arctic haze, mercury and the chemical composition of snow across northwestern Alaska. *Atmos. Environ.* **38**, 805–820 (2004).
- Reynolds, R. L. *et al.* Composition of dust deposited to snow cover in the Wasatch Range (Utah, USA): Controls on radiative properties of snow cover and comparison to some dust-source sediments. *Aeolian Res.* **15**, 73–90 (2014).
- Dong, Z., Qin, D., Qin, X., Cui, J. & Kang, S. Changes in precipitating snow chemistry with seasonality in the remote Laohuguo glacier basin, western Qilian Mountains. *Environ. Sci. Pollut. R.* **24**(12), 11404–11414 (2017).
- Dong, Z. *et al.* Individual particles of cryoconite deposited on the mountain glaciers of the Tibetan Plateau: Insights into chemical composition and sources. *Atmos. Environ.* **138**, 114–124 (2016).
- Gao, Y., Yang, C., Ma, J. & Yin, M. Characteristics of the trace elements and arsenic, iodine and bromine species in snow in east-central China. *Atmos. Environ.* **174**, 43–53 (2018).
- Damdinsuren, B. & Kawai, J. Variation of trace elements in snow during starting and ending of snowfall in Kyoto city measured by low power total reflection X-ray fluorescence spectrometry. *X Ray Spectrom.* **47**, 273–276 (2018).
- Ginot, P., Kull, C., Schwikowski, M., Schotterer, U. & Gäggeler, H. W. Effects of postdepositional processes on snow composition of a subtropical glacier (Cerro Tapado, Chilean Andes). *J. Geophys. Res. Atmos.* **106**(D23), 32375–32386 (2001).
- Sinclair, K. E. & MacDonell, S. Seasonal evolution of penitente glaciochemistry at Tapado Glacier, Northern Chile. *Hydrol. Process.* **30**, 176–186 (2016).
- Cereceda-Balic, F. *et al.* Impact of Santiago de Chile urban atmospheric pollution on anthropogenic trace elements enrichment in snow precipitation at Cerro Colorado, Central Andes. *Atmos. Environ.* **47**, 51–57 (2012).
- Toro, R. *et al.* Exploring atmospheric stagnation during a severe particulate meter air pollution episode over complex terrain in Santiago, Chile. *Environ. Pollut.* **244**, 705–714 (2019).
- Cordero, R. R. *et al.* Aerosol Effect on the UV Irradiance in Santiago de Chile. *Atmos. Res.* **149**, 282–291 (2014).
- Cortés, G., Giroto, M. & Margulis, S. A. Analysis of sub-pixel snow and ice extent over the extratropical Andes using spectral unmixing of historical Landsat imagery. *Remote Sens. Environ.* **141**, 64–78 (2014).
- Cortés, G., Giroto, M. & Margulis, S. A. Snow process estimation over the extratropical Andes using a data assimilation framework integrating MERRA data and Landsat imagery. *Water Resour. Res.* **52**, 2582–2600 (2016).
- Saavedra, F. A., Kampf, S. K., Fassnacht, S. R. & Sibold, J. S. A snow climatology of the Andes Mountains from MODIS snow cover data. *Int. J. Climatol.* **37**, 1526–1539 (2017).
- Garreaud, R. & Aceituno, P. Atmospheric circulation over South America: mean features and variability in *The Physical Geography of South America* (eds Veblen, T. K. Orme, A. R. & Young, K.) (Oxford University Press, 2007).
- Garreaud, R. The Andes climate and weather. *Adv. Geosci.* **7**, 1–9 (2009).
- Stehr, A. & Aguayo, M. Snow cover dynamics in Andean watersheds of Chile (32.0–39.5°S) during the years 2000–2016. *Hydrol. Earth Syst. Sci.* **21**, 5111–5126 (2017).
- Russell, A. M., Gnanadesikan, A. & Zaitchik, B. Are the Central Andes Mountains a Warming Hot Spot? *J. Clim.* **30**, 3589–3608 (2017).
- Garreaud, R. *et al.* The 2010–2015 megadrought in central Chile: impacts on regional hydroclimate and vegetation. *Hydrol. Earth Syst. Sci. Discuss.* **21**, 6307–6327 (2017).
- Boisier, J. P., Rondanelli, R., Garreaud, R. D. & Muñoz, F. Anthropogenic and natural contributions to the Southeast Pacific precipitation decline and recent megadrought in Central Chile. *Geophys. Res. Lett.* **43**, 413–421 (2016).
- Rowe, P. M. *et al.* Black carbon and other light-absorbing impurities in snow in the Chilean Andes. *Sci. Rep.* **9**(1), 4008 (2019).
- Córdova, A. M. *et al.* On the transport of urban pollution in an Andean mountain valley. *Aerosol Air Qual. Res.* **16**, 593–605 (2016).
- de Solminihac, H., Gonzales, L. E. & Cerda, R. Copper mining productivity: lessons from Chile. *J. Policy Model.* **40**, 182–193 (2018).
- Molina, C., Toro, R., Morales, R. G. E., Manzano, C. & Leiva-Guzman, M. A. Particulate matter in urban areas of south-central Chile exceeds air quality standards. *Air Qual. Atmos. Health* **10**, 653–667 (2017).

30. Stewart, C. *et al.* Contamination of water supplies by volcanic ashfall: A literature review and simple impact modelling. *J. Volcanol. Geotherm. Res.* **158**, 296–306 (2006).
31. Venzke, E. *Volcanoes of the World*, v. 4.7.5. *Global Volcanism Program*, <https://doi.org/10.5479/si.GVP.VOTW4-2013> (2013)
32. Aguilera, F. *et al.* Eruptive activity of Peteroa Volcano for period 2010–2011, Southern Volcanic Zone, Chile. *Andean Geol.* **43**, 20–46 (2016).
33. Doherty, S. J. *et al.* Observed vertical redistribution of black carbon and other insoluble light-absorbing particles in melting snow. *J. Geophys. Res. Atmos.* **118**, 5553–5569 (2013).
34. Determination of Metals in Ambient Particulate Matter Using X-ray Fluorescence (XRF) Spectroscopy - Compendium of Methods for the Determination of Inorganic Compounds in Ambient Air Compendium Method IO-3.3; EPA/625/R-96/010a; U.S. Environmental Protection Agency: Cincinnati, OH, <http://www.epa.gov/ttnamti1/files/ambient/inorganic/mthd-3-3.pdf> (1999).
35. Kang, C. M., Achilleos, S., Lawrence, J., Wolfson, J. M. & Koutrakis, P. Interlab comparison of elemental analysis for low ambient urban PM<sub>2.5</sub> levels. *Environ. Sci. & Technol.* **48**, 12150–12156 (2014).
36. Moore, D. M., & Reynolds, R. C. *X-ray Diffraction and the Identification and Analysis of Clay Minerals* (Vol. 322, p. 321). (Oxford university Press, 1989).
37. Reimann, C., Filzmoser, P. & Garrett, R. G. Factor analysis applied to regional geochemical data: problems and possibilities. *Appl. Geochem.* **17**, 185–206 (2002).
38. Statsoft, Inc. *STATISTICA (data analysis software system), version 7*, [www.statsoft.com](http://www.statsoft.com) (2018).
39. Carling, G. T., Fernandez, D. P. & Johnson, W. P. Dust-mediated loading of trace and major elements to Wasatch Mountain snowpack. *Sci. Total Environ.* **432**, 65–77 (2012).
40. Dong, Z. *et al.* New insights into trace elements deposition in the snow packs at remote alpine glaciers in the northern Tibetan Plateau, China. *Sci. Total Environ.* **529**, 101–113 (2015).
41. Cantonati, M. *et al.* Achnanthidium minutissimum (Bacillariophyta) valve deformities as indicators of metal enrichment in diverse widely-distributed freshwater habitats. *Sci. Total Environ.* **475**, 201–215 (2014).
42. Veyseyre, A. *et al.* Heavy metals in fresh snow collected at different altitudes in the Chamonix and Maurienne Valleys, French Alps: initial results. *Atmos. Environ.* **35**, 415–425 (2001).
43. Veinott, G., Perron-Cashman, S. & Anderson, M. R. Baseline metal concentrations in coastal Labrador sediments. *Mar. Pollut. Bull.* **42**, 187–192 (2001).
44. Birkeland, P. W. In *Soils and geomorphology. Third edition* (ed. Birkeland, P. W.) 239–278 (Oxford University Press, 1999).
45. Casalino, C. A., Malandrino, M., Giacomino, A. & Abollino, O. Total and fractionation metal contents obtained with sequential extraction procedures in a sediment core from Terra Nova Bay, West Antarctica. *Antarc. Sci.* **25**, 83–98 (2013).
46. Alfonso, J. A. *et al.* Geochemistry of recent lacustrine sediments from Fildes Peninsula, King George Island, maritime Antarctica. *Antarc. Sci.* **27**, 462–471 (2015).
47. Draxler, R. R. & Hess, G. D. An overview of the HYSPLIT\_4 modelling system for trajectories, dispersion and deposition. *Aust. Meteorol. Mag.* **47**, 295–308 (1998).
48. Draxler, R. R. & Rolph, G. D. HYSPLIT (HYbrid Single-Particle Lagrangian Integrated Trajectory) Model access via NOAA ARL READY Website, <http://ready.arl.noaa.gov/HYSPLIT.php>. NOAA Air Resources Laboratory, Silver Spring, MD (2015).
49. Stein, A. F. *et al.* NOAA's HYSPLIT atmospheric transport and dispersion modeling system. *Bull. Amer.* **96**, 2059–2077 (2015).
50. NOAA Air Resources Laboratory (ARL), Global Data Assimilation System (GDAS1) Archive Information. Tech. rep, <http://ready.arl.noaa.gov/gdas1.php> (2004).
51. Su, L., Yuan, Z., Fung, J. C. & Lau, A. K. A comparison of HYSPLIT backward trajectories generated from two GDAS datasets. *Sci. Total Environ.* **506**, 527–537 (2015).
52. Sillitoe, R. H. Space-time distribution. Crustal setting and Cu/Mo ratios of central Andean porphyry copper deposits: Metallogenic implications in Geology and metallogeny of copper deposits in *Geology and Metallogeny of Copper Deposits* (eds Friedrich, G. H. *et al.*) 235–250 (Springer-Verlag Berlin Heidelberg, 1986).
53. Sanchez-Alfaro, P. *et al.* Physical, chemical and mineralogical evolution of the Tolhuaca geothermal system, southern Andes, Chile: Insights into the interplay between hydrothermal alteration and brittle deformation. *J. Volcanol. Geotherm. Res.* **324**, 88–104 (2016).
54. Wrage, J. *et al.* Geochemistry of thermal waters in the southern volcanic zone, Chile – implications for structural controls on geothermal fluid composition. *Chem. Geol.* **466**, 545–561 (2017).
55. Pokrovski, G. S., Borisova, A. Y. & Bychkov, A. Y. Speciation and transport of metals and metalloids in geological vapors. *Rev. Mineral. Geochem.* **76**, 165–218 (2013).
56. Allard, P. *et al.* Acid gas and metal emission rates during long-lived basalt degassing at Stromboli volcano. *Geophys. Res. Lett.* **27**, 1207–1210 (2000).
57. Borisova, A. Y., Pokrovski, G. S., Pichavant, M., Freyrier, R. & Candaudap, F. Arsenic enrichment in hydrous peraluminous melts: Insights from femtosecond laser ablation-inductively coupled plasma-quadrupole mass spectrometry, and *in situ* X-ray absorption fine structure spectroscopy. *Am. Min.* **95**, 1095–1104 (2010).
58. Bia, G., Borgnino, L., Gaiero, D. & Garcia, M. G. Arsenic-bearing phases in South Andean volcanic ashes: Implications for As mobility in aquatic environments. *Chemical Geology* **393**, 26–35 (2015).
59. Naranjo, J. A. & Moreno, H. Actividad explosiva postglacial en el Volcán Llaima, Andes del Sur (38°45'S). *Rev. Geol. Chil.* **18**, 69–80 (1991).
60. Ruggieri, F. *et al.* Environmental geochemistry of recent volcanic ashes from the Southern Andes. *Environ. Chem.* **8**, 236–247 (2011).
61. Roquer, T. *et al.* Fault-controlled development of shallow hydrothermal systems: Structural and mineralogical insights from the southern Andes. *Geotherm.* **66**, 156–173 (2017).
62. Hunter, J. D. Matplotlib: A 2D graphics environment. *Comput. Sci. Eng.* **9**(3), 90–95 (2007).
63. Wang, Y. Q. Meteoinfo: GIS software for meteorological data visualization and analysis. *Meteorol. Appl.* **21**, 360–368 (2014).

## Acknowledgements

The support of the Consejo Nacional de Ciencias y Tecnología (CONICYT, Preis ANILLO ACT1410, FONDECYT 1161460, FONDECYT 1171690 and FONDECYT 1191932), The Instituto Antártico Chileno (INACH, Preis RT\_32–15), the Corporación de Fomento de la Producción (CORFO, Preis 18BPE-93920, 18BPCR-89100, 17BPE-73748, & 16BPE2-66227), and the Universidad de Santiago de Chile (Preis USA1555), is gratefully acknowledged. We are grateful to Francisca Quiroz, Juan Rayas, Camilo Guzman, Christian Brahm, Catalina Pino, Pedro Marconi, Nicole Torres, Marta Caballero, Andrea Sepúlveda and Dr. Delia Rodríguez, who participated in snow sampling. S.N. was supported by NSF grant CHE-1306366, by a Lantz Senior Sabbatical Fellowship from the University of Puget Sound, and by the Fulbright Scholar program. We thank the National Oceanic and Atmospheric Administration (NOAA) for the Global Data Assimilation System (GDAS1) Archive Information provided through the Real-time Environmental Applications and Display sYstem (READY) (<http://ready.arl.noaa.gov/gdas1.php>).

### Author Contributions

Conceived and designed the experiments: R.R.C., P.M.R., S.N., G.C., J.C., F.L., J.P., A.D. and S.F. Performed the experiments: F.F., J.J., S.M., B.G., J.M.C., J.F., P.L. and E.S. Analyzed the data: J.A.A., R.R.C., P.O., C.M.K. and B.G. Wrote the paper: J.A.A., R.R.C., S.M., A.D., S.N. and S.F.

### Additional Information

**Supplementary information** accompanies this paper at <https://doi.org/10.1038/s41598-019-44516-5>.

**Competing Interests:** The authors declare no competing interests.

**Publisher's note:** Springer Nature remains neutral with regard to jurisdictional claims in published maps and institutional affiliations.



**Open Access** This article is licensed under a Creative Commons Attribution 4.0 International License, which permits use, sharing, adaptation, distribution and reproduction in any medium or format, as long as you give appropriate credit to the original author(s) and the source, provide a link to the Creative Commons license, and indicate if changes were made. The images or other third party material in this article are included in the article's Creative Commons license, unless indicated otherwise in a credit line to the material. If material is not included in the article's Creative Commons license and your intended use is not permitted by statutory regulation or exceeds the permitted use, you will need to obtain permission directly from the copyright holder. To view a copy of this license, visit <http://creativecommons.org/licenses/by/4.0/>.

© The Author(s) 2019